INTERPRETABILITY OF RIEMANNIAN TOOLS USED IN BRAIN COMPUTER INTERFACES

Thibault de Surrel[⋆] *Tristan Venot*[†] *Marie-Constance Corsi*[†] *Florian Yger*[‡]

[⋆] LAMSADE, CNRS, PSL Univ. Paris-Dauphine, France
[†] Sorbonne Université, Institut du Cerveau - Paris Brain Institute - ICM, CNRS, Inria, Inserm, AP-HP, Hôpital de la Pitié Salpêtrière, Paris, France
[‡] LITIS, INSA Rouen-Normandy, France

ABSTRACT

Riemannian methods have established themselves as state-of-the-art approaches in Brain-Computer Interfaces (BCI) in terms of performance. However, their adoption by experimenters is often hindered by a lack of interpretability. In this work, we propose a set of tools designed to enhance practitioners' understanding of the decisions made by Riemannian methods. Specifically, we develop techniques to quantify and visualize the influence of the different sensors on classification outcomes. Our approach includes a visualization tool for high-dimensional covariance matrices, a classifier-agnostic tool that focuses on the classification process, as well as methods that leverage the data's topology to better characterize the role of each sensor. We demonstrate these tools on a specific dataset and provide Python code to facilitate their use by practitioners, thereby promoting the adoption of Riemannian methods in BCI.

***Index Terms*—** Interpretability, Riemannian geometry, Brain Computer Interfaces, ElectroEncephaloGram

1. INTRODUCTION

Controlling a device through the modulation of the brain activity is an absolute challenge, especially when using non-invasive techniques such as electroencephalography (EEG). Brain Computer Interfaces (BCI) [1] rely on the acquisition of users' brain signals, their conversion into commands, and the provision of feedbacks to users to inform them about their mental states in real time. The challenge stems from the various sources of variability, which lead 15–30% of BCI users to be unable to control a BCI device even after several training sessions [2, 3, 4]. Among these sources of variability are the quality of the signal (e.g. signal-to-noise ratio), and some intrinsic characteristics of the BCI experiment itself. Indeed, a standard pipeline typically involves extracting features from EEG signals—sometimes neurophysiologically relevant ones—and feeding them into a machine learning algorithm. This leads to sources of uncertainties in the outcome that can hinder the feedback to subjects. With discriminant signals stable in time, those sources of uncertainty would not be an issue. Unfortunately, this is not the case in the context of motor imagery (MI) based BCI which rely on the imagination of a movement without performing it. Indeed, the difficulty of this task generates different types of variability [5, 6]: i) *inter-subject variability*: the mental task is performed differently by the different subjects; ii) *intra-subject variability*: changes across time can be observed due to the signals drift or to fluctuations of the neural signatures because of the subjects' fatigue or difficulty in performing the tasks in a robust

Subject	MDM Score	Class	Riem. Variance
1	0.84 ± 0.02	Left hand	11.20
		Right hand	10.01
2	0.49 ± 0.04	Left hand	17.44
		Right hand	16.22
3	0.93 ± 0.03	Left hand	24.71
		Right hand	20.56
4	0.68 ± 0.10	Left hand	10.24
		Right hand	11.93
5	0.54 ± 0.07	Left hand	14.55
		Right hand	13.17
6	0.66 ± 0.07	Left hand	18.44
		Right hand	22.06
7	0.71 ± 0.14	Left hand	12.85
		Right hand	12.01
8	0.95 ± 0.02	Left hand	15.02
		Right hand	15.10
9	0.77 ± 0.04	Left hand	24.66
		Right hand	30.73

Table 1: Performance of the MDM classifier per subject and class on the dataset BNCI2014-001. The Riemannian variance is reported for each class.

This work was funded by the French National Research Agency for project PROTEUS (grant ANR-22-CE33-0015-01). We also acknowledge support from the European Research Council, Grant Agreement No. 864729

979-8-3503-2411-2/25/$31.00 ©2025 IEEE

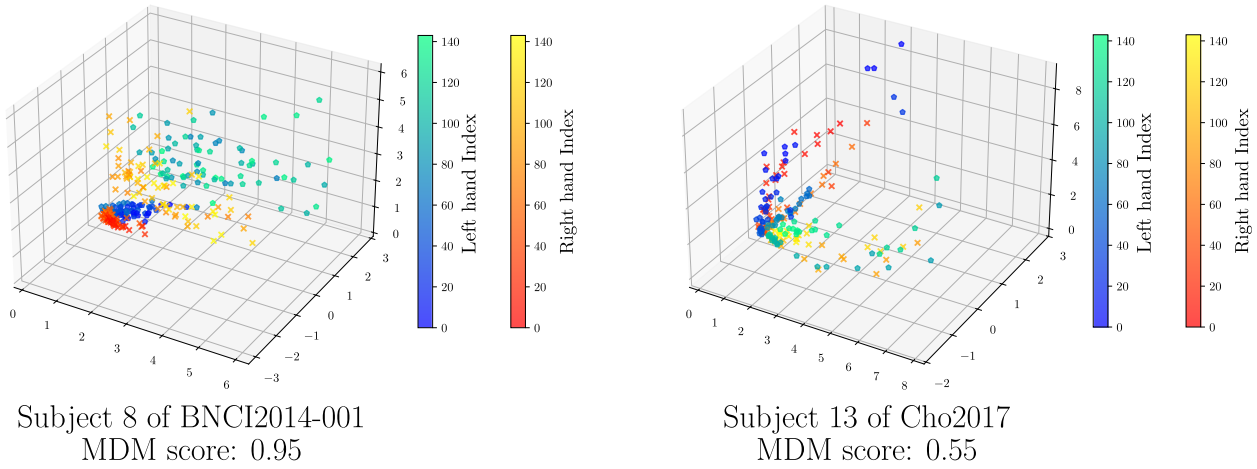

Subject 8 of BNCI2014-001
MDM score: 0.95

Subject 13 of Cho2017
MDM score: 0.55

Fig. 1: t-SNE visualization of subject 8 of BNCI2014-001 and of subject 13 of Cho2017. Each point represents a 2×2 covariance matrix. The shape of the markers and the colormaps correspond to the two classes (`left_hand` and `right_hand`). Given a class (therefore a colormap), the color is chosen as the time index of recording of the corresponding EEG.

way. MI-based BCI [7] usually rely on the use of power spectra features, exploiting the Event Related Desynchronization/ Synchronization (ERD/ERS) [8] effect that occur in certain frequency bands (α 8-12 Hz, β 13-30 Hz [9]). The ERD/S effect consists in the local (the sensori motor regions) decrease (Desynchronization) of power spectral density and in the increase (Synchronization) in the α and β bands with respect to a baseline test. These features appear to vary over time for most subjects, even when task performance remains high, suggesting a performance plateau that may result from the current features capturing only local and incomplete information [10]. In recent years, Riemannian geometry based algorithms completely obliterated the competition regarding BCI scores. These Riemannian methods use as main feature the covariance matrix, and leverage the mathematical structure of the latter to yield better results [11]. Indeed, a covariance matrix is a *Symmetric Positive Definite* (SPD) matrix, inducing a non-flat Riemannian structure where the curvature plays a critical role. These Riemannian algorithms are mainly more robust to noise [12], and therefore became the state of the art in the classification of EEG data for BCI. Unfortunately, the Riemannian approach cannot be linked directly to what is known from a neurophysiological perspective, mainly because the covariance matrix is not inherently interpretable. A reduced number of works proposed to select more relevant subsets of channels based on the Riemannian classification [13], but those works were meant to improve the classification results and not to serve as support for interpretation. Indeed, it is necessary to develop tools to explain why these Riemannian methods perform well at classifying MI tasks from a neurophysiological perspective—both at the feature level and at the classification level—in the same way it is possible with ERD/ERS. Here, we propose original approaches suited for Riemannian geometry methods from the features' perspective (the covariance matrices) and agnostic to the classifier which show both temporal and spatial interpretations. Being able to interpret Riemannian classifiers could help uncovering potential "Clever Hans" phenomena [14] and eliminate potential biases in data. Those tools would help the BCI community in adopting with more trust the Riemannian approach meaning we could access to the best performing algorithm while knowing that they can be neurophysiologically explained. All the tools presented in the following are available on a GitHub repository[1], to ease their adoption by the community.

2. VISUALIZATION OF COVARIANCE DATASETS

When dealing with new datasets to classify, a classical first step consists in exploring the features by visualizing them to see if they are differentiable [15]. Such a step is also important to provide some insights on the brain signatures associated with the task performance. When the objects of interest are covariance matrices, one problem in visualizing them is their high dimensionality. Indeed, the EEG is recorded using C sensors, so the associated covariance matrix is of size $C \times C$. When $C > 2$ (which is often the case in BCI), one cannot visualize the set of covariance matrices. To solve this issue, we use a Riemannian version of the t-SNE algorithm proposed in [16]. This tool enables the user to reduce the dimension of covariance matrices (and more generally SPD matrices) to 2×2 SPD matrices while taking into account the Riemannian geometry of SPD matrices. These low dimensional SPD matrices can be plotted in 3D, as a 2×2 SPD

[1] `https://github.com/thibaultdesurrel/influence_channel`

matrix is of the following form:

$$X = \begin{pmatrix} a & b \\ b & c \end{pmatrix}$$

where $a > 0, c > 0$ and $ac > b^2$. The symmetry of these matrices lead to a 3 dimensional space and X can therefore be represented in $\mathbb{R}^3$ using the coordinates (a, b, c). One can then plot the set of covariance matrices of a particular subject and try to understand what is going on. Moreover, if one knows the recording order of the EEGs, one can also visualize the temporal evolution of the covariance matrices using a colormap for example. We did this for the subject 8 of the dataset BNCI2014-001 [17] and the subject 13 of the dataset Cho2017 [18]. The resulting 3D plots are given at fig. 1. In these plots, we show two different things. First, the two colormaps correspond to the two classes (`left_hand` and `right_hand`). According to table 1, we know that subject 8 of BNCI2014-001 has a high classification score (0.95 ± 0.02). We therefore expect the classes to be well separated in the t-SNE visualization. We recall that the t-SNE has no class information during its fitting. This is what we observe in the left plot of fig. 1, as it seems that the two colormaps are in different areas of the plots. On the contrary, subject 13 of Cho2017 has a very bad classification score (0.55 ± 0.04) and we can indeed see in the right plot of fig. 1 that the two colormaps are completely mixed up. Therefore, we have a coherent result between the t-SNE visualizations and the *a posteriori* classification results. We also plot a second information, given a class (therefore a colormap), the color is chosen as the index of recording of the corresponding EEG. Therefore, if we focus on the left hand, the greener the points are, the latter in the session they were recorded. We can thus see the evolution of the mind state of the subject during the experiment. For subject 8 of BNCI2014-001 (the plot on the left of fig. 1), the dataset was recorded during two separated sessions. This is visible as the points (in each class) seem to be separated in two clusters: a red/blue one and a yellow/green one. Those two clusters actually correspond to the two sessions.

Such a visualization technique could also be used to understand and illustrate the strategy employed by a user to generate a given command, or to detect drifts in the data. Additionally, it could serve as feedback during the calibration phase or throughout user training.

3. CONTRIBUTION OF AN ELECTRODE TO THE FRÉCHET VARIANCE

The previous tool presents the advantage of reducing the dimension while showing the separability between classes and through time. However, spatial interpretation is still needed to establish a link with the sensorimotor areas involved in motor imagery tasks. The purpose of the second tool we propose here is two-fold: i) to identify the resulting variability of the feature in its class and ii) to link it to its spatial origin. Moreover, this tool can be confronted to the initial ERD/ERS criterion of separability as they both capture related information.

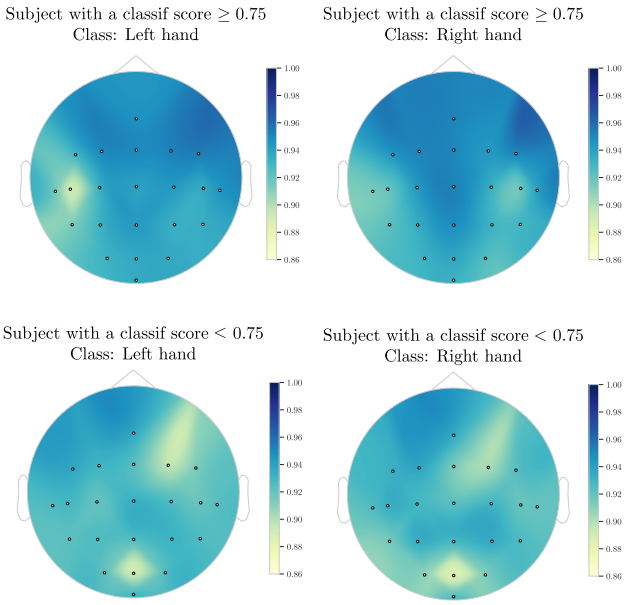

Fig. 2: Mean of the influence of each sensor on the Riemannian variance. Dataset: BNCI2014-001 [17]. The ratio between the variance of the "partial" covariance matrices and the "full" ones is plotted here. The darker the color is, the more variance this sensor brings and the lighter the color, the less variance is brought by this sensor. The top row corresponds to subjects with a classification score ≥ 0.75 and the bottom one to the other subjects.

We propose a method to measure the variance brought by a sensors (without knowing if this variance is brought by noise or by useful information). For this, let us recall that given a set of covariance matrices $(X_i)_{i=1,...,N}$, one can compute its Riemannian mean [19] $\bar{X}$ as the point that minimizes the squared Riemannian distances to each X_i:

$$\bar{X} \in \underset{X \in \mathcal{P}_C}{\operatorname{argmin}} \frac{1}{N} \sum_{i=1}^{N} \delta(X_i, X)^2. \quad (1)$$

where $\mathcal{P}_C$ is the set of $C \times C$ SPD matrices. Then, one can compute the Riemannian variance, denoted σ^2, that corresponds to the minimum attained in eq. (1):

$$\sigma^2 = \frac{1}{N} \sum_{i=1}^{N} \delta(X_i, \bar{X})^2.$$

Let us denote $(X_i)_{i=1,...,N}$ the set of *full* covariance matrices computed with all the sensors. It is a set of $C \times C$ SPD matrices, where C is the number of channels. Then, for $c \in \{1, ..., C\}$, let us denote $(X_i^{(-c)})_{i=1,...,N}$ the set of *partial* covariance matrices computed after removing channel c. These matrices are therefore of dimension $(C-1) \times (C-1)$ and corresponds to the set $(X_i)_{i=1,...,N}$ where we have removed the c-th line and the c-th column. We can compare

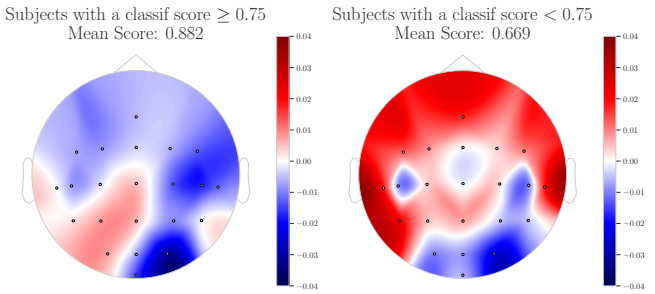

Fig. 3: Mean of the influence of each sensor on the classification using an MDM. Dataset: BNCI2014-001 [17]. The relative error between the score of an MDM trained with the "partial" covariance matrices and the "full" ones is plotted here for each sensors. The bluer the color, the most useful the sensors are for the classification. The right plot corresponds to subjects with a classification score ≥ 0.75 and the left one to the other subjects.

the "full" Riemannian variance $\sigma^{2,\text{full}}$ computed using the set of full covariance matrices $(X_i)_i$ and the "partial" Riemannian variance $\sigma^{2,(-c)}$ computed using the set of partial covariance matrices $(X_i^{(-c)})_i$, themselves computed after removing channel c. To compare them, we compute their ratio:

$$\frac{\sigma^{2,(-c)}}{\sigma^{2,\text{full}}}.$$

Such a measure is interpreted as follows: it shows how much information would be lost if a given electrode were removed. The information is not necessarily related to the class information as some sensors could bring the same amount of information in each class (and would not be useful for classification purposes) but would be related to some underlying cognitive mechanisms at play in the brain. We can compute this ratio of variances of all sensors and plot them on a topographic map. This ratio is interesting to look at per class, meaning that we consider only the covariance matrices of a given class, and then of the other. We do this on the BNCI2014-001 dataset, providing the mean topographic maps for subjects with classification scores above and below 0.75 (see table 1). The topographic maps are given at fig. 2.

4. CONTRIBUTION OF AN ELECTRODE TO THE CLASSIFICATION

Once the features fed to the classifiers have been evaluated, we can assess whether those that align with a neurophysiological explanation yield the best classification performance in terms of accuracy. Moreover, we can investigate whether the performances are aligned with the ERD/ERS criterion. Here, subjects that presented high level of desynchronization were found to have good performances using Riemannian classifiers. However, some subjects that would have been discarded based solely on ERD/ERS considerations still exhibited good performances. A tool is therefore needed to know if this difference is purely based on a non-explainable sensitivity of the classifier, or if it can be traced back to a neurophysiological explanation (meaning here that sensorimotor regions are the primary source of information of the classifier).

In order to do this, we want to analyze the influence of the sensors on the Riemannian classification of covariance matrices. We will use the same setup as in section 3 by comparing the classification score when considering the "full" covariance matrices or when considering the "reduced" one. Given a Riemannian classifier (such as the *Minimum Distance to Mean* (MDM) or the *Tangent Space LDA* (TS-LDA) [12]), one can train it using the set of "full" covariance matrices $(X_i)_{i=1,\dots,N}$ or using the set of "partial" covariance matrices $(X_i^{(-c)})_{i=1,\dots,N}$. We can then compare the score s^{full} of the "full" classifier and the score $s^{(-c)}$ for the "partial" classifier by computing their relative error:

$$\frac{s^{(-c)} - s^{\text{full}}}{s^{\text{full}}}.$$

As this gives us one value per sensor, we can plot all the relative errors using a topographic map. An important point of this tool is that it is *classifier agnostic*, meaning that one can plug any Riemannian classifier. In fig. 3, we do it for the classifier MDM on the dataset BNCI2014-001. We plot the mean topographic maps for the subjects with a classification score that is greater than 0.75 and for the subjects with a classification score that is less than 0.75 (based on table 1). When the relative error is greater than zero (the areas in red in the plot), this means that removing the sensors improves the classifier whereas when the relative error is less than zero (the blue areas), this indicates that removing the sensors decreases the classification score. We can see that most of the sensors, for the subjects with a classification accuracy of over 75%, are in blue, meaning that they all bring useful information to the classifier and that removing them deteriorates the classification accuracy. Moreover, for the subjects with an accuracy that is less than 75%, most sensors are in red, meaning that they most likely bring some noise to the signal and removing them improves the classification. Nevertheless, for all subjects, the sensors C3 and C4, are very useful as they are in blue. This is coherent as the motor imagery actions were `left_hand` versus `right_hand` and the sensors C3 and C4 are the ones that capture this information. Therefore, the important information for the Riemannian point of view is the same as from a neurophysiological point of view. However, for the subjects with an accuracy over 75%, some sensors seem to be important from a Riemannian perspective even if it would not be the case neurophysiologically. For example, the sensors at the back of the head (P2, Pz, POz) are positioned over the visual cortex. Therefore, neurophysiologically, they would be less prone to provide relevant information regarding the classification of `left_hand` versus `right_hand`. However, from a Riemannian point of view, it

seems that they bring useful information for the classification, as removing them worsen the results. A possible explanation is that the Riemannian classifiers behaves as a "clever Hans" and uses some signals triggered by the visual cue shown to the subject to indicate which action to mentally perform.

5. CONCLUSION

In this work, we propose different tools of visualization and explanation tailored for Riemannian geometry approaches over Brain Computer Interface EEG data. These tools make it possible to evaluate the relevance of the features processed by classification algorithms, in order to understand where class separation occurs, both at the feature level and at the classification level. We exploited tools that reduced the covariance matrix to low dimensional SPD matrices while providing the temporal evolution. Furthermore, we provided a tool to visualize the spatial variability intra-class (*via* the Riemannian variance) which can be exploited to understand the underlying neurophysiological process. Finally, we could evaluate spatially the contribution of each sensor to the accuracy of the classification which allows a post classification check on the relevance of the choice made by the classifier. There is increasing interest in interpretability at the different steps of BCI pipelines as they are becoming more and more sophisticated especially with the integration of deep learning to the classification part [20, 21].

Some limitations must be acknowledged. First, the t-SNE method is purely a visualization tool, no properties over the covariance matrices can be retrieved from it; moreover, the stochastic component makes the visualization variable. On another note, the variance method is still difficult to interpret especially at the level of the full covariance matrix as it could be linked to other observations. This suggests further inquiries on its interpretability. Another limit of our visualizations is that they do not provide any insights on the error bars or subject-level variabilities. Some work could be carried out on developing new ways of visualizing the data produced by our methods. Nevertheless, this work constitutes a first proof-of-concept. Indeed, the representation of the covariance matrices makes it very difficult to assess their variation in time. By eliciting the trials, we can track covariance evolution across time which is crucial to understand how our features shift from the beginning to the end of the session. To increase their diffusion, those implementations need to be validated on more BCI paradigms, not only on motor imagery based BCI. P300 speller for instance is a BCI that detects the P300 event-related potential -a spike $\sim 300ms$ after a target stimulus- to select characters on a grid by flashing rows and columns [22, 23]. Another method is SSVEP, a BCI method where the user focuses on a flickering stimulus at a known frequency, and the system detects matching frequency components in the EEG to infer user intent [24]. Those tools were mainly designed for an offline use, to investigate the data after it has been collected. However, in a logic of BCI experimentation integration, they could be added to already existing pipelines that help in the decision process over features selection to train on for online setups. Then, the computational complexity of these tools should be studied in more depth. Those pipelines could then be integrated into dedicated software such as HappyFeat [25] (an open-source software package designed for real-time EEG feature extraction and classification) and used in experience settings. From another perspective, the use case presented here only relied on covariance matrix as the initial computation step on EEG. Nevertheless, other estimators can provide SPD matrices. Functional connectivity matrices estimated on coherence, imaginary coherence [26] or even avalanche transition matrices [27] could be used. As they have been studied more in depth on their neurophysiological signatures, the Riemannian tools applied to them could find more echoes on their results [28]. Finally, it is clear that the application of Riemannian approaches could extend beyond BCI experiments. When it comes to EEG data, the tools presented here could also be useful in the context of brain monitoring or diagnosis, as they provide clear metrics on the data processed by complex classifiers.

6. REFERENCES

[1] M. Clerc, L. Bougrain, and F. Lotte, *Les interfaces cerveau-ordinateur 2: technologie et applications*, ISTE Group, 2016.

[2] B. Allison and C. Neuper, "Could anyone use a BCI?," in *Brain-Computer Interfaces: Applying our Minds to Human-Computer Interaction*, Desney S. Tan and Anton Nijholt, Eds., Human-Computer Interaction Series, pp. 35–54. Springer, 2020.

[3] S. Becker, K. Dhindsa, L. Mousapour, and Y. Al Dabagh, "BCI illiteracy: It's us, not them. optimizing BCIs for individual brains," in *2022 10th International Winter Conference on Brain-Computer Interface (BCI)*, 2022, pp. 1–3, ISSN: 2572-7672.

[4] M. Lee, O. Kwon, Y. Kim, H. Kim, Y. Lee, J. Williamson, S. Fazli, and S. Lee, "EEG dataset and OpenBMI toolbox for three BCI paradigms: an investigation into BCI illiteracy," *GigaScience*, vol. 8, no. 5, pp. giz002, 2019.

[5] H. Hwang, C. Im, and S. Park, "Evaluation of feature extraction methods for motor imagery-based bcis in terms of robustness to slight changes of electrode locations," in *2013 International Winter Workshop on Brain-Computer Interface (BCI)*, 2013, pp. 76–78.

[6] K.-R. Müller, "Analysing the changing brain: Immediate brain plasticity after one hour of BCI," in *2020 8th International Winter Conference on Brain-Computer Interface (BCI)*, 2020, pp. 1–2, ISSN: 2572-7672.

[7] G. Pfurtscheller and C. Neuper, "Motor imagery and direct brain-computer communication," *Proceedings of the IEEE*, vol. 89, no. 7, pp. 1123–1134, 2001, Conference Name: Proceedings of the IEEE.

[8] G. Pfurtscheller and F. H. Lopes da Silva, "Event-related EEG/MEG synchronization and desynchronization: basic principles," *Clinical Neurophysiology: Official Journal of the International Federation of Clinical Neurophysiology*, vol. 110, no. 11, pp. 1842–1857, 1999.

[9] J. A. Simpson and W. Fitch, "Chapter 16 - the electroencephalogram," in *Applied Neurophysiology*, J. A. Simpson and W. Fitch, Eds., pp. 147–153. Butterworth-Heinemann, 1988.

[10] J. D. Wander, T. Blakely, K. J. Miller, K. E. Weaver, L. A. Johnson, J. D. Olson, E. E. Fetz, R. P. N. Rao, and J. G. Ojemann, "Distributed cortical adaptation during learning of a brain–computer interface task," *Proceedings of the National Academy of Sciences*, vol. 110, no. 26, pp. 10818–10823, 2013, Publisher: Proceedings of the National Academy of Sciences.

[11] F. Yger, M. Berar, and F. Lotte, "Riemannian Approaches in Brain-Computer Interfaces: A Review," *IEEE Trans. Neural Syst. Rehabil. Eng.*, vol. 25, no. 10, pp. 1753–1762, Oct. 2017.

[12] A. Barachant, S. Bonnet, M. Congedo, and C. Jutten, "Multiclass Brain–Computer Interface Classification by Riemannian Geometry," *IEEE Transactions on Biomedical Engineering*, vol. 59, no. 4, pp. 920–928, Apr. 2012.

[13] A. Barachant and S. Bonnet, "Channel selection procedure using riemannian distance for BCI applications," in *2011 5th International IEEE/EMBS Conference on Neural Engineering*, 2011, pp. 348–351, ISSN: 1948-3554.

[14] S. Lapuschkin, S. Wäldchen, A. Binder, G. Montavon, W. Samek, and K. Müller, "Unmasking clever hans predictors and assessing what machines really learn," *Nature communications*, vol. 10, no. 1, pp. 1096, 2019.

[15] L Vega-Escobar, AE Castro-Ospina, and L Duque-Muñoz, "Feature extraction schemes for bci systems," in *STSIVA*. IEEE, 2015, pp. 1–6.

[16] T. de Surrel, S. Chevallier, F. Lotte, and F. Yger, "Geometry-aware visualization of high dimensional symmetric positive definite matrices," *TMLR*, 2025.

[17] M Tangermann, K-R. Müller, A. Aertsen, N. Birbaumer, C. Braun, C. Brunner, R. Leeb, C. Mehring, K. Miller, G. Mueller-Putz, G. Nolte, G. Pfurtscheller, H. Preissl, G. Schalk, A. Schlögl, C. Vidaurre, S. Waldert, and B. Blankertz, "Review of the bci competition iv," *Frontiers in Neuroscience*, vol. 6, 2012.

[18] H. Cho, M. Ahn, S. Ahn, M. Kwon, and S. Jun, "EEG datasets for motor imagery brain–computer interface," *GigaScience*, vol. 6, no. 7, pp. gix034, May 2017.

[19] M. Moakher, "A Differential Geometric Approach to the Geometric Mean of Symmetric Positive-Definite Matrices," *SIAM J. Matrix Anal. Appl.*, vol. 26, no. 3, pp. 735–747, Jan. 2005.

[20] F. Lotte, L. Bougrain, A. Cichocki, M. Clerc, M. Congedo, A. Rakotomamonjy, and F. Yger, "A review of classification algorithms for EEG-based brain–computer interfaces: a 10 year update," *J. Neural Eng.*, vol. 15, no. 3, pp. 031005, 2018.

[21] X. Zhang, L. Yao, X. Wang, J. Monaghan, D. McAlpine, and Y. Zhang, "A survey on deep learning-based non-invasive brain signals: recent advances and new frontiers," *J. Neural Eng.*, vol. 18, no. 3, 2021.

[22] D. Brandeis and D. Lehmann, "Event-related potentials of the brain and cognitive processes: Approaches and applications," *Neuropsychologia*, vol. 24, no. 1, pp. 151–168, 1986.

[23] J. Pan, X. Chen, N. Ban, J. He, J. Chen, and H. Huang, "Advances in p300 brain–computer interface spellers: toward paradigm design and performance evaluation," *Frontiers in Human Neuroscience*, vol. 16, 2022.

[24] C. Guger, B. Allison, B. Grosswindhager, R. Prückl, C. Hintermüller, C. Kapeller, M. Bruckner, G. Krausz, and G. Edlinger, "How many people could use an SSVEP BCI?," *Frontiers in Neuroscience*, vol. 6, 2012.

[25] A. Desbois, A. Venot, F. De Vico Fallani, and M-C. Corsi, "*HappyFeat*—an interactive and efficient BCI framework for clinical applications," *Software Impacts*, vol. 19, pp. 100610, 2024.

[26] G. Nolte, O. Bai, L. Wheaton, Z. Mari, S. Vorbach, and M. Hallett, "Identifying true brain interaction from EEG data using the imaginary part of coherency," *Clinical Neurophysiology: Official Journal of the International Federation of Clinical Neurophysiology*, vol. 115, no. 10, pp. 2292–2307, 2004.

[27] M-C. Corsi, P. Sorrentino, D. Schwartz, N. George, L. L. Gollo, S. Chevallier, L. Hugueville, A. E. Kahn, S. Dupont, D. S. Bassett, V. Jirsa, and F. De Vico Fallani, "Measuring neuronal avalanches to inform brain-computer interfaces," *iScience*, vol. 27, no. 1, pp. 108734, 2024.

[28] M-C. Corsi, S. Chevallier, F. De Vico Fallani, and F. Yger, "Functional connectivity ensemble method to enhance BCI performance (FUCONE)," *IEEE Trans Biomed Eng*, vol. 69, no. 9, pp. 2826–2838, 2022.